



Research Article

Di Lin*, Yutong Feng, Zhengqi Ren and David J. Richardson

The generation of femtosecond optical vortex beams with megawatt powers directly from a fiber based Mamyshev oscillator

<https://doi.org/10.1515/nanoph-2021-0537>

Received September 16, 2021; accepted November 2, 2021;

published online November 11, 2021

Abstract: Numerous approaches have been developed to generate optical vortex beams carrying orbital angular momentum (OAM) over the past decades, but the direct intracavity generation of such beams with practical output powers in the femtosecond regime still remains a challenge. Here we propose and experimentally demonstrate the efficient generation of high-peak-power femtosecond optical vortex pulses from a Mamyshev oscillator (MO) based on few-mode polarization-maintaining (PM) ytterbium-doped fibers (YDFs). By employing an appropriate intracavity transverse spatial mode selection technique, ultrafast pulses carrying OAM with selectable topological charge of $l = \pm 1$ are successfully generated with an average output power of ~ 5.72 W at ~ 24.35 MHz repetition rate, corresponding to a single pulse energy of ~ 235 nJ. The chirped pulses can be compressed to ~ 76 fs outside the cavity, leading to a pulse peak power of ~ 2.2 MW. To the best of our knowledge, this is by far the highest pulse energy and peak power for optical vortex pulses ever generated directly from a fiber oscillator. This unprecedented level of performance should be of great interest for a variety of applications including materials processing and imaging.

Keywords: Mamyshev oscillator; mode-locked fiber laser; optical vortex beam; ultrafast pulse generation.

1 Introduction

Optical vortex beams are characterized by an annular intensity profile associated with an azimuthally varying phase structure of $\exp(il\varphi)$ (where l is the integer of topological charge) and that carry OAM of $l\hbar$ per photon (where \hbar is Planck's constant). Such beams are subject to ever increasing attention due to their relevance and potential for widespread practical application in areas such as optical communications [1, 2], high resolution microscopy [3, 4], quantum information [5], macro-/nano-particle manipulation [6, 7] and material processing [8, 9]. Normally, such beams are generated by taking the Gaussian-profiled output beam from a laser and applying a helical phase front external to the laser cavity using a suitable spatial beam shaper – typically either a spiral phase plate [10], phase-only spatial light modulator [11], q -plate [12] or optical metasurface [13]. This approach works well and can be applied to both continuous-wave and pulsed lasers. However, there are often drawbacks associated with this external-cavity approach due to the power handling capabilities, modal purity, overall mode conversion loss and topological charge dispersion associated with these various beam shaping devices. These become of particular concern for the efficient generation of high average power and high peak power femtosecond optical vortex beams with their associated high intensities and broad spectral bandwidth.

The generation of optical vortex beams directly from a laser cavity generally relies on the excitation of particular eigenmodes such as higher-order Laguerre–Gaussian (LG) modes in free space cavities and Bessel modes in cavities based on circularly symmetric optical waveguides such as fibers. This therefore offers the potential for the generation of beams with high modal purity by exploiting spatial mode competition within a laser cavity. Moreover, by placing the shaping element within high gain cavities at locations in which the circulating power is much lower than the output beam power the risk of laser induced damage can be reduced. This strategy can also be used to minimize the impact of the loss of the beam shaping

*Corresponding author: Di Lin, Optoelectronics Research Centre, University of Southampton, Southampton, SO17 1BJ, UK, E-mail: di.lin@soton.ac.uk. <https://orcid.org/0000-0001-5025-9051>
Yutong Feng, Zhengqi Ren and David J. Richardson, Optoelectronics Research Centre, University of Southampton, Southampton, SO17 1BJ, UK. <https://orcid.org/0000-0002-6839-2106> (Y. Feng)

element on the final shaped beam power/overall laser efficiency. Many intracavity beam shaping results have been reported in recent years, both from solid state bulk [14–17] and fiber oscillators [18–20]. Compared with bulk solid-state lasers, fiber lasers offer benefits in terms of higher wall-plug efficiencies, greater compactness and robustness and lower cost. Moreover, through the use of cladding-pumping, they are well suitable for high average output power operation.

Although a few techniques have been demonstrated for the generation of femtosecond optical vortex pulses from mode-locked (ML) fiber lasers, these have generally relied on the generation of traditional soliton pulses within a single mode fiber (SMF) oscillator in combination with a mode converter (e.g. a mode-selective coupler [21], two-mode long-period fiber grating [22], an acoustically induced fiber grating [23], or q -plate [24]) placed just before the output coupler, allowing the circulating Gaussian-shaped beam to be converted to an OAM beam in the process of being coupled out of the cavity. This underlying approach is therefore largely equivalent in practical terms to extra-cavity beam shaping and therefore it intrinsically suffers from the same drawbacks mentioned previously. The average output power of the generated femtosecond OAM beams based on such lasers is usually limited to a few tens of mW with maximum pulse energies of a few nJ and pulse durations down to a few hundred fs by the mode-locking mechanisms so far employed in these shaping experiments. However, there has been recent progress on increasing the output energy from ML fiber lasers. Using the MO concept Z. Liu et al. demonstrated that sub-50 fs pulses with a pulse energy of ~ 50 nJ could be obtained directly from an SMF based ML fiber MO, representing a significant increase in achievable pulse energy relative to prior approaches [25]. Following this initial demonstration the pulse energy has been further scaled up to ~ 625 nJ from an MO based on use of the fundamental mode in a step-index, few mode PM-YDF with a high quality, single mode Gaussian-shaped output beam obtained [26]. In addition, it is to be noted that few-mode step-index YDFs have also previously been successfully employed as the gain medium for directly generating/amplifying optical vortex and vector beams in various fiber laser and amplifier systems [18, 27, 28]. Here amplification in higher-order modes has been used to achieve up to 106 W of average output power and ~ 180 kW of peak power for picosecond pulses [27]. The benefits of the larger mode area in terms of increased extractable pulse energy and reduced nonlinearity due to the increased mode area of the higher order modes versus the fundamental mode of the fiber were observed.

The observations above provide the incentive to explore the possibility of developing a few-mode fiber based MO with the capability to generate femtosecond optical vortex pulses with much higher pulse energy and higher average output power than the current state-of-the-art and in this paper we report the efficient generation of femtosecond optical vortex pulses with controllable topological charge of $l = \pm 1$ from a ring cavity MO using a few-mode PM-YDF. A q -plate combined with a pair of quarter-wave plates (QWPs) is employed within the cavity to convert the linearly polarized fundamental mode (LP_{01}) from the first arm of the MO into a linearly polarized OAM mode that is then amplified in the second arm. A large fraction of the amplified OAM mode is coupled out of the cavity, and the residual is converted back to the LP_{01} mode which is then fed back to the first arm. The laser provides up to ~ 5.72 W of average output power at a slope efficiency of $\sim 73\%$ for a pulse repetition rate of ~ 24.35 MHz, corresponding to a single pulse energy of ~ 235 nJ. The chirped output pulses are compressed down to ~ 76 fs in an external grating compressor leading to ~ 2.2 MW peak powers in the final optical vortex beams.

2 Principles

In a weakly guided circular core few-mode PM fiber, the strong linear birefringence breaks the circular symmetry of the fiber eigenmodes, leading to linearly polarized fiber eigenmodes that are approximately equivalent to the familiar LP modes. We therefore designate the PM fiber eigenmodes as LP_{lme} and LP_{lmo} , where l and m are the azimuthal and radial indices, respectively. The birefringence substantially lifts the difference in effective refractive index ($\Delta n_{\text{eff}} > 10^{-4}$) of the LP_{lm} modes between the orthogonal linear polarizations, while the LP_{lme} and LP_{lmo} modes with the same linear polarization are still nearly degenerate due to the relatively small Δn_{eff} (10^{-5} – 10^{-7}). The linearly polarized OAM modes in a PM fiber can be considered as coherent superpositions of the same linearly polarized even and odd LP_{lm} modes with $\pm\pi/2$ phase shift, as illustrated in Figure 1. The generation of stable linearly polarized OAM modes with controllable topological charge has recently been demonstrated in passive PM fibers [29–31]. Compared with non-PM fibers, the reduced number of nearly degenerate modes in PM fibers reduces mode coupling and leads to relatively stable OAM modes. The Δn_{eff} between the even and odd LP_{11} modes with the same polarization in a few-mode PM fiber with a core diameter of $25 \mu\text{m}$ and a numerical aperture (NA) of 0.065 is calculated to be $\sim 2 \times 10^{-7}$ (using the COMSOL Finite Element Method

between them is expected even in the case of small external perturbations. To reduce the mode coupling and to ensure the effective amplification of the first-order OAM modes within the fiber, the PM-YDF in the second arm was only loosely coiled with a large bending diameter of ~ 30 cm, and any twisting of the fiber was avoided. The second arm is backward cladding pumped by a 50 W multimode 975 nm laser diode using free space coupling optics. All fiber ends of the PM-YDFs were spliced to appropriate silica endcaps with a diameter of ~ 250 μm which were polished with an angle of $\sim 8^\circ$ to suppress the potential for any parasitic lasing.

Two reflective ruled diffraction gratings (Thorlabs, GR25-0303) with groove densities of 300 lines/mm in combination with SMFs form the offset bandpass filters required within the MO, each offering Gaussian-shaped spectral transmission profiles – one with a center wavelength set at 1042 nm with a 2.2 nm full-width at half-maximum (FWHM), and the other at 1030 nm with a 1.7 nm FWHM passband. The large spectral separation between the two filters leads to a high modulation depth for the effective saturable absorber response they provide and this allows high energy pulses to be stabilized. The combination of the HWP and the PBS in each arm is used to provide adjustable output coupling. We minimized the output coupling ratio in the first arm to ensure the signal power seeded into the second arm is as high as possible, and the output coupling ratio of the second arm was set to $\sim 95\%$ to maximize the energy of the output pulses. The combination of a pair of QWPs and a q -plate with appropriate rotation angles forms an OAM beam converter that converts a linearly polarized Gaussian-shaped beam into a linearly polarized OAM beam with a controllable topological charge of $l = \pm 1$, or vice versa [15]. The q -plate (Thorlabs WPV10L-1064) has a high transmittance of $\sim 98\%$ around 1 μm and a laser damage threshold of 5 W/cm for continuous wave operation. Taking the theoretical mode conversion efficiency of $\sim 93\%$ into account, the overall mode conversion efficiency is $\sim 91\%$. Although the q -plate is designed to provide half-wavelength retardance at 1064 nm, we previously employed it to convert a Gaussian-shaped beam into a radially polarized beam for picosecond pulses at a center wavelength of 1035 nm, resulting in a pronounced donut-shaped intensity profile with negligible intensity at the beam center in the far-field, which is critical for amplifying a donut-shaped mode in a fiber as any residual intensity at the beam center will be amplified significantly due to the very high gain at the center of fiber core and which is not accessible by a donut-shaped beam [27]. One beam converter is placed just before the PM-YDF of the second arm to convert the incident linearly polarized

Gaussian-shaped beam emitted from the first arm into a linearly polarized OAM beam that is then coupled to the few-mode PM-YDF in order to excite the linearly polarized OAM mode within this fiber. The benefits of such a configuration are obvious. On the one hand, placing the beam converter prior to a gain fiber in which the powers are relatively low, allows the pre-shaped beam to be amplified to the desired beam with much higher output power than could be safely applied from a damage perspective directly to the beam converter external to the cavity. On the other hand, it also avoids any shaping losses and minimizes the impact of topological dispersion. Behind the output coupler of the second arm, the other OAM beam converter in combination with a short length of SMF forms a spatial mode correlation filter providing a transmission function that has a conjugate phase to the desired OAM mode and that consequently passes light in the desired linearly polarized OAM mode whilst strongly attenuating light in all other unwanted modes [32, 33]. A free-space polarization independent isolator ensures unidirectional operation (clockwise).

4 Experimental results

To initiate the mode-locking, an external seed beam emitted from an in-house-built, dispersion-managed SMF ML oscillator is employed. The output pulses are first compressed to ~ 300 fs and then coupled to a 2 m length of SMF to increase the spectral bandwidth (-10 dB level) to ~ 30 nm and that extends over the passbands of the two intracavity spectral filters. Chirped pulses with an energy of ~ 5 pJ at a repetition rate of 23.15 MHz were launched in to the first arm through the fiber tap. The repetition rate of the seed pulse has a negligible effect on initiating mode-locking as reported in [25]. However, the pulse energy of the seed is a critical parameter in initiating mode-locking. A seed with too high a pulse energy would lead to amplification of the seed itself, while a seed with too low an energy would not enable sufficient spectral broadening to enable pulses to circulate through the full cascade of amplifiers within the cavity. After optimizing the seed/circulating signal launch conditions into the few-mode PM-YDF in the second arm and carefully manipulating the few-mode PM-YDF to reduce the inter-modal coupling, mode-locking with a donut-shaped OAM output beam can be repeatedly and reliably initiated at a fundamental repetition rate of ~ 24.35 MHz when the absorbed pump power is above ~ 6.9 W. We observed that the mode-locking always operated within the single pulse regime above the mode-lock threshold, which is mainly due to the relatively high

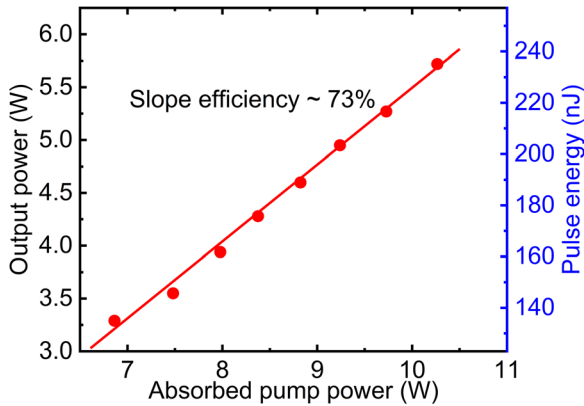


Figure 3: The output power and pulse energy as a function of absorbed pump power.

intracavity loss induced by the high output coupling ratio and effective intracavity spatial mode filtering. Once mode-locking was initiated we blocked the seed and gradually increased the pump power in the second arm while keeping the pump power in the first arm constant. Figure 3 shows the average output power and pulse energy of the generated ML OAM pulses as a function of the absorbed pump power in the second arm. The average output power

reached a maximum of 5.72 W with a slope efficiency of $\sim 73\%$ with respect to the absorbed pump power in the second arm, corresponding to a maximum pulse energy of ~ 235 nJ. We monitored to ensure that an almost constant pulse energy of ~ 1.5 nJ of signal was coupled to the second arm (~ 1.5 dB coupling loss was measured), indicating that the second arm provided a maximum effective gain of ~ 22 dB.

Figure 4(a) shows a typical measured ML pulse train with a repetition rate of ~ 24.35 MHz, which is in agreement with calculations based on the cavity length and highlights the very good stability achieved. The stability of the output pulse train was further investigated using a radio frequency (RF) spectrum analyzer. As shown in Figure 4(b), the RF spectrum was recorded with a span window of 100 kHz and a 10 Hz resolution bandwidth (RBW). It shows that the fundamental beat mode has a signal-to-noise ratio of ~ 70 dB, indicating highly stable mode-locking with comparable performance to more conventional ML SMF oscillators. The narrow peak also indicates relatively low amplitude fluctuation. The inset of Figure 4(b) shows the recorded RF spectrum with a span of 1 GHz and an RBW of 10 kHz, showing no sign of multiple pulsing. It is worth mentioning that the oscillator can stably operate in the

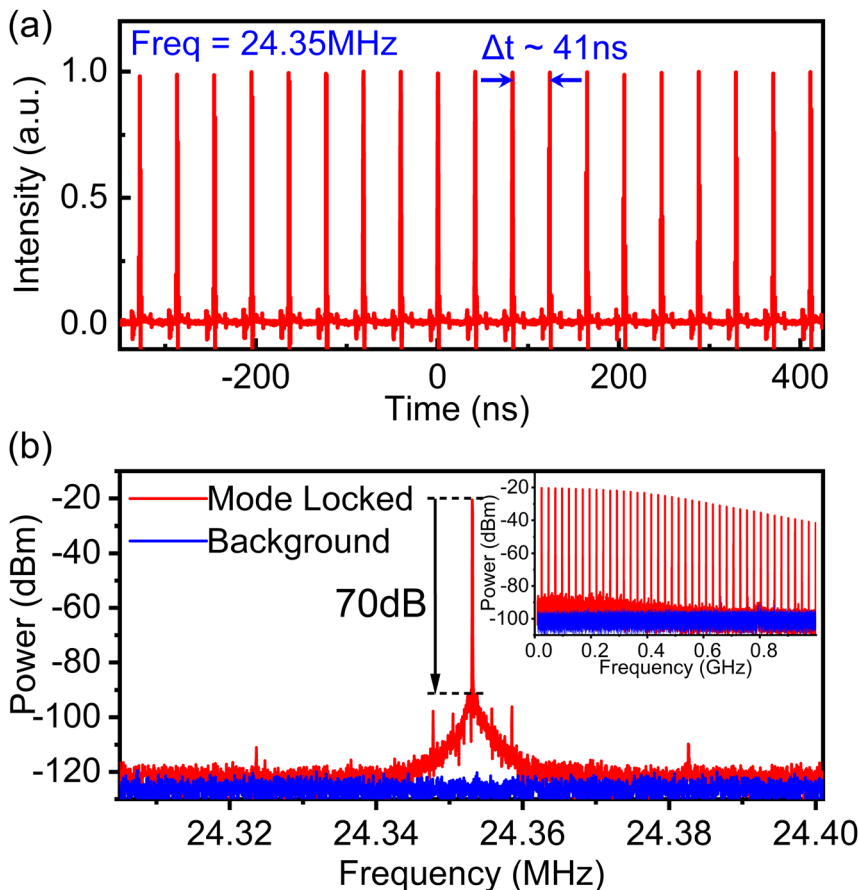


Figure 4: (a) Measured output pulse train. (b) Radio frequency spectrum with a RBW of 10Hz and a span of 200kHz at the fundamental frequency of 24.35MHz. Inset: RF spectrum with 1GHz span.

mode-locking state with negligible variation in the donut-shaped intensity profile and a fixed topological charge for periods in excess of at least 2 h in a typical laboratory environment.

Figure 5(a) shows the output spectra directly measured after the output coupler of the second arm for different pulse energies. The spectra are as one would expect for self-phase modulation (SPM)-broadening of almost unchirped Gaussian pulses [34]. The bandwidth at the -10 dB level increases from ~ 40 nm to ~ 60 nm (ranging from 1010 nm to 1070 nm) as the pulse energy increases from 145 nJ to 235 nJ. The spectra exhibit asymmetric profiles due mainly to the self-steepening effect and pulse distortions due to third-order dispersion. The intensity autocorrelation (AC) duration of the chirped output pulses was measured to be ~ 2.8 ps. The output pulses were successfully compressed using a pair of transmission gratings (1000 lines/mm) with a compression efficiency of $\sim 72\%$, resulting in a

maximum compressed pulse energy of ~ 169 nJ. We observed that the AC duration of the compressed pulses decreased with an increase in the pulse energy. The duration of the AC trace of the compressed pulse was measured to ~ 107 fs (FWHM) at the maximum pulse energy as shown in the red curve in Figure 5(b), which is reasonably well fitted with the calculated AC trace for a Gaussian-shaped pulse as shown in the blue-dash curves. The calculated TL pulse has an AC duration of ~ 79 fs as shown by the black curve, which is ~ 1.35 times shorter than the measured pulse. Assuming a Gaussian pulse shape, the temporal duration of the compressed pulses in the OAM beam is estimated to ~ 76 fs with a peak power of ~ 2.2 MW. The deviation between the measured and the TL AC duration can be attributed to higher order phase induced by nonlinear effects and the grating compressor itself. The clean and single peak AC trace measured with a long range (64 ps) delay window is shown in the inset of Figure 5 excludes the existence of any broad pedestal underneath the signal and potential multiple pulses.

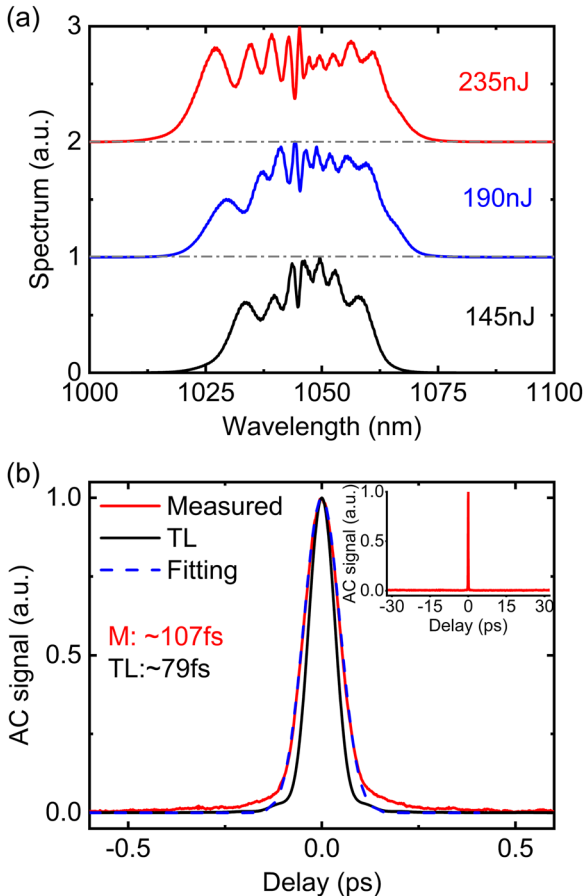


Figure 5: (a) Experimentally measured spectra with increasing pulse energy. (b) The measured AC trace (red curve) of the compressed pulse at the maximum pulse energy of 235 nJ and the comparison with the Gaussian-fit (blue dash curve) and the calculated AC trace of the transform-limited (TL) pulse (black curve). Inset: The measured intensity AC trace with 60 ps span.

Figure 6(a) and (b) show typical spatial intensity distributions for the output OAM beams with opposite handedness of helical phase front measured at the maximum output power, respectively. Both beams show a pronounced donut-shaped pattern. The slight deviation from an ideal donut-shape can be attributed to a slight power imbalance between the orthogonal LP_{11e} and LP_{11o} modes resulting from residual inter-modal coupling. The OAM mode purity was measured to $\sim 93\%$ with the mode decomposition method as described in [33]. Figure 6(c) and (d) show the measured interference patterns of the corresponding output beams presented in Figure 6(a) and (b), respectively. The spiral fringes with opposite rotation directions confirm the opposite topological charge of the helical phase front for the generated OAM beams. The change of topological charge of OAM beams was simply achieved by rotating the fast axes of the QWPs in both beam converters by 90° (which required that the mode-locking be re-initiated). It is worth mentioning that the output OAM beam can sometimes exhibit a degree of beam distortion as a result of susceptibility to mode coupling between the orthogonal LP_{11e} and LP_{11o} modes due to perturbations, (primarily bend and thermally induced), during the propagation and amplification through the fiber due to the relatively small Δn_{eff} . However, we found that it was possible to optimise the quality (e.g. cylindrical symmetry) of the donut intensity profile of the output beam by applying a controlled level of stress to the PM-YDF in the horizontal plane in order to adjust the relative weighting and phase between these two orthogonal modes. This had no impact at all on the handedness of the helical phase

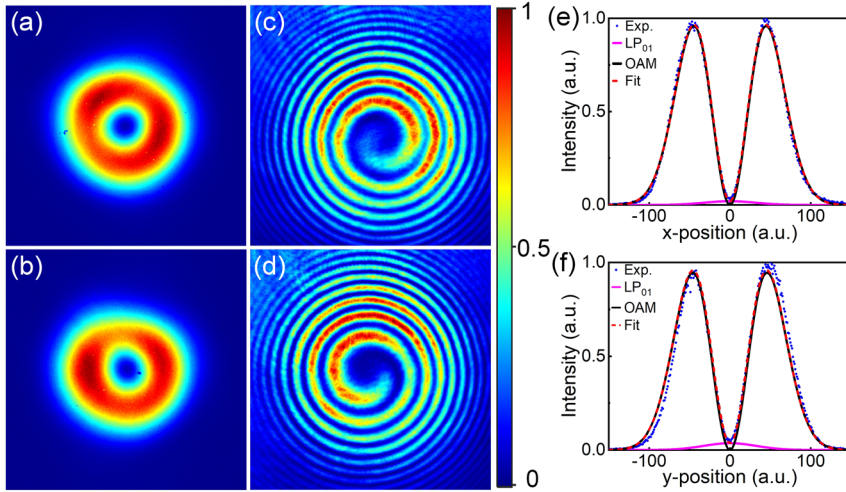


Figure 6: Measured far-field intensity distributions for the generated OAM beams with topological charge of (a) $l=1$ and (b) $l=-1$; (c) and (d) interference patterns of the corresponding beams; intensity distribution across the beam center along (e) horizontal and (d) vertical axis corresponding to the beams in (a) and (b), respectively. The blue dot curves are the measured intensity profiles, the solid dark curves and solid pink curves represent the theoretical intensity profiles of the OAM mode ($|l|=1$) and LP_{01} modes, respectively; the short dash red curves represent the incoherent superposition of the intensity profiles of the LP_{01} and OAM modes.

front. The blue dots in Figure 6(e) and (f) show the measured one-dimensional intensity distributions across the center of the beams shown in Figure 6(a) and (b) along the x -position and y -position, respectively. It is clear that there is some low level residual intensity at the center of the beam which we believe to be due to amplified spontaneous emission (ASE) within the fundamental LP_{01} mode. The measured intensity profiles can be fitted well with incoherent intensity superposition of the fundamental Gaussian mode (LG_{00}) and the first-order ($|l|=1$) OAM mode (namely the first higher-order Laguerre–Gaussian mode (LG_{01}) in free-space, represented by the red short-dash curves). The power weighting of the OAM mode is calculated to $> \sim 98.6\%$. We observed that any further increase in the absorbed pump power beyond ~ 10.8 W would significantly increase the power in the LP_{01} mode and hence result in unstable mode-locking and that eventually mode-locking would be suddenly lost once the threshold for parasitic lasing on the fundamental LP_{01} mode was exceeded. We believe this to be the main reason we were unable to further scale the pulse energy of our OAM pulses.

5 Conclusions

In summary, we have proposed and demonstrated a novel approach to efficiently generate high energy femtosecond OAM pulses with controllable topological charges of $l = \pm 1$ directly from a ring-cavity ML fiber MO based on commercially available few-mode PM-YDFs. The generated optical vortex pulses are formed from the coherent superpositions of the two linearly polarized LP_{11o} and LP_{11e} fiber eigenmodes with $\pm\pi/2$ relative phase shift. The experimental results indicate that the relative phase between the orthogonal LP modes can be maintained even in the

presence of very strong nonlinearly induced spectral broadening, resulting in OAM pulses with high peak power and high modal purity. The MO reaches an average output power of ~ 5.72 W at a repetition rate of 24.35 MHz, corresponding to a single pulse energy of ~ 235 nJ. The generated OAM pulses have a spectra bandwidth of ~ 60 nm at the -10 dB level and can be dechirped external to the cavity to achieve pulses with an AC duration of ~ 107 fs. Assuming a Gaussian-shaped pulse, the temporal width of the OAM pulses is estimated to ~ 76 fs, leading to an estimated peak power of ~ 2.2 MW. The maximum ML output power is mainly limited by the build-up of ASE in the fundamental LP_{01} mode and ultimately parasitic lasing. This might be improved by using more sophisticated bulk end-caps to better suppress parasitic lasing and/or by more advanced fibers which have a ring-shaped Yb-doping profile. The demonstrated ultrafast OAM pulse generation and power-handling capabilities of our approach opens a new pathway to the generation of high peak power, high average output power ultrashort OAM pulses from simple and compact fiber oscillators. The laser may prove useful for a wide range of applications including laser-based material processing and high-resolution medical imaging.

Acknowledgements: We thank Radan Slavik, Meng Ding and Zitong Feng for providing the RF spectrum analyzer and discussions on RF spectral measurement.

Author contribution: D. L. conceived the idea and performed the experiments with assistance from Y. F. and Z. R.; D. L. and D. J. R. wrote the paper with inputs from all co-authors; D. J. R. supervised the project.

Research funding: Engineering and Physical Sciences Research Council (EPSRC) (EP/P030181/1; EP/N00762X/1; EP/P027644/1).

Conflict of interest statement: The authors declare no conflicts of interest regarding this article.

Data availability: All source data supporting this study are openly available from the University of Southampton Repository (<https://doi.org/10.5258/SOTON/D2023>).

References

- [1] J. Wang, J. Y. Yang, I. M. Fazal, et al., “Terabit free-space data transmission employing orbital angular momentum multiplexing,” *Nat. Photonics*, vol. 6, pp. 488–496, 2012.
- [2] N. Bozinovic, Y. Yue, Y. X. Ren, et al., “Terabit-scale orbital angular momentum mode division multiplexing in fibers,” *Science*, vol. 340, pp. 1545–1548, 2013.
- [3] S. W. Hell and J. Wichmann, “Breaking the diffraction resolution limit by stimulated emission: stimulated-emission-depletion fluorescence microscopy,” *Opt. Lett.*, vol. 19, pp. 780–782, 1994.
- [4] S. Furchapter, A. Jesacher, S. Bernet, and M. Ritsch-Marte, “Spiral phase contrast imaging in microscopy,” *Opt. Express*, vol. 13, pp. 689–694, 2005.
- [5] A. Mair, A. Vaziri, G. Weihs, and A. Zeilinger, “Entanglement of the orbital angular momentum states of photons,” *Nature*, vol. 412, pp. 313–316, 2001.
- [6] D. G. Grier, “A revolution in optical manipulation,” *Nature*, vol. 424, pp. 810–816, 2003.
- [7] M. Padgett and R. Bowman, “Tweezers with a twist,” *Nat. Photonics*, vol. 5, pp. 343–348, 2011.
- [8] D. Flamm, D. G. Grossmann, M. Sailer, et al., “Structured light for ultrafast laser micro- and nanoprocessing,” *Opt. Eng.*, vol. 60, 2021, <https://doi.org/10.1117/1.oe.60.2.025105>.
- [9] J. J. Nivas, S. T. He, A. Rubano, et al., “Direct femtosecond laser surface structuring with optical vortex beams generated by a q-plate,” *Sci. Rep.*, vol. 5, p. 17929, 2015.
- [10] M. W. Beijersbergen, R. P. C. Coerwinkel, M. Kristensen, and J. P. Woerdman, “Helical-wavefront laser beams produced with a spiral phaseplate,” *Opt. Commun.*, vol. 112, pp. 321–327, 1994.
- [11] G. Gibson, J. Courtial, M. Padgett, et al., “Free-space information transfer using light beams carrying orbital angular momentum,” *Opt. Express*, vol. 12, pp. 5448–5456, 2004.
- [12] L. Marrucci, C. Manzo, and D. Paparo, “Optical spin-to-orbital angular momentum conversion in inhomogeneous anisotropic media,” *Phys. Rev. Lett.*, vol. 96, p. 163905, 2006.
- [13] R. C. Devlin, A. Ambrosio, N. A. Rubin, J. P. B. Mueller, and F. Capasso, “Arbitrary spin-to-orbital angular momentum conversion of light,” *Science*, vol. 358, pp. 896–900, 2017.
- [14] D. Lin, J. M. O. Daniel, and W. A. Clarkson, “Controlling the handedness of directly excited Laguerre-Gaussian modes in a solid-state laser,” *Opt. Lett.*, vol. 39, pp. 3903–3906, 2014.
- [15] D. Naidoo, F. S. Roux, A. Dudley, et al., “Controlled generation of higher-order Poincare sphere beams from a laser,” *Nat. Photonics*, vol. 10, pp. 327–333, 2016.
- [16] D. J. Kim and J. W. Kim, “Direct generation of an optical vortex beam in a single-frequency Nd:YVO₄ laser,” *Opt. Lett.*, vol. 40, pp. 399–402, 2015.
- [17] J. T. Fan, J. Zhao, L. P. Shi, N. Xiao, and M. L. Hu, “Two-channel, dual-beam-mode, wavelength-tunable femtosecond optical parametric oscillator,” *Adv Photonics*, vol. 2, p. 1, 2020.
- [18] D. Lin and W. A. Clarkson, “Polarization-dependent transverse mode selection in an Yb-doped fiber laser,” *Opt. Lett.*, vol. 40, pp. 498–501, 2015.
- [19] Y. Tanaka, M. Okida, K. Miyamoto, and T. Omatsu, “High power picosecond vortex laser based on a large-mode-area fiber amplifier,” *Opt. Express*, vol. 17, pp. 14362–14366, 2009.
- [20] D. Lin, J. M. O. Daniel, M. Gecevicius, M. Beresna, P. G. Kazansky, and W. A. Clarkson, “Cladding-pumped ytterbium-doped fiber laser with radially polarized output,” *Opt. Lett.*, vol. 39, pp. 5359–5361, 2014.
- [21] T. Wang, F. Wang, F. Shi, et al., “Generation of femtosecond optical vortex beams in all-fiber mode-locked fiber laser using mode selective coupler,” *J. Lightwave Technol.*, vol. 35, pp. 2161–2166, 2017.
- [22] R. S. Chen, F. L. Sun, J. N. Yao, et al., “Mode-locked all-fiber laser generating optical vortex pulses with tunable repetition rate,” *Appl. Phys. Lett.*, vol. 112, p. 261103, 2018.
- [23] W. D. Zhang, K. Y. Wei, D. Mao, et al., “Generation of femtosecond optical vortex pulse in fiber based on an acoustically induced fiber grating,” *Opt. Lett.*, vol. 42, pp. 454–457, 2017.
- [24] K. Huang, J. Zeng, J. W. Gan, Q. Hao, and H. P. Zeng, “Controlled generation of ultrafast vector vortex beams from a mode-locked fiber laser,” *Opt. Lett.*, vol. 43, pp. 3933–3936, 2018.
- [25] Z. W. Liu, Z. M. Ziegler, L. G. Wright, and F. W. Wise, “Megawatt peak power from a Mamyshev oscillator,” *Optica*, vol. 4, pp. 649–654, 2017.
- [26] D. Lin, D. Xu, J. He, Y. Feng, Z. Ren, and D. J. Richardson, “Generation of ~625 nJ pulses from a Mamyshev oscillator with a few-mode LMA Yb-doped fiber,” in *2021 Conference on Lasers and Electro-Optics Europe and European Quantum Electronics Conference*, OSA Technical Digest (Optical Society of America, 2021), 2021, p. cj_4_4. Available at: https://www.osapublishing.org/abstract.cfm?uri=CLEO_Europe-2021-cj_4_4.
- [27] D. Lin, N. Baktash, S. U. Alam, and D. J. Richardson, “106 W, picosecond Yb-doped fiber MOPA system with a radially polarized output beam,” *Opt. Lett.*, vol. 43, pp. 4957–4960, 2018.
- [28] D. Lin, J. Carpenter, Y. T. Feng, Y. M. Jung, S. U. Alam, and D. J. Richardson, “High-power, electronically controlled source of user-defined vortex and vector light beams based on a few-mode fiber amplifier,” *Photon. Res.*, vol. 9, pp. 856–864, 2021.
- [29] R. D. Niederriter, M. E. Siemens, and J. T. Gopinath, “Simultaneous control of orbital angular momentum and beam profile in two-mode polarization-maintaining fiber,” *Opt. Lett.*, vol. 41, pp. 5736–5739, 2016.
- [30] R. D. Niederriter, M. E. Siemens, and J. T. Gopinath, “Continuously tunable orbital angular momentum generation using a polarization-maintaining fiber,” *Opt. Lett.*, vol. 41, pp. 3213–3216, 2016.
- [31] Z. P. Dong, Y. M. Zhang, H. X. Li, et al., “Generation of stable orbital angular momentum beams with an all-polarization-maintaining fiber structure,” *Opt. Express*, vol. 28, pp. 9988–9995, 2020.
- [32] T. Kaiser, D. Flamm, S. Schroter, and M. Duparre, “Complete modal decomposition for optical fibers using CGH-based correlation filters,” *Opt. Express*, vol. 17, pp. 9347–9356, 2009.
- [33] D. Lin, J. Carpenter, Y. T. Feng, et al., “Reconfigurable structured light generation in a multicore fibre amplifier,” *Nat. Commun.*, vol. 11, p. 3986, 2020.
- [34] R. H. Stolen and C. Lin, “Self-phase-modulation in silica optical fibers,” *Phys. Rev. A*, vol. 17, pp. 1448–1453, 1978.